Contrib Mineral Petrol (2005) 150: 251–267
DOI 10.1007/s00410-005-0673-8

ORIGINAL PAPER

D. R. Bell · M. Grégoire · T. L. Grove · N. Chatterjee
R. W. Carlson · P. R. Buseck

# Silica and volatile-element metasomatism of Archean mantle: a xenolith-scale example from the Kaapvaal Craton

Received: 23 June 2004 / Accepted: 30 March 2005 / Published online: 6 September 2005
© Springer-Verlag 2005

**Abstract** Textural evidence in a composite garnet harzburgite mantle xenolith from Kimberley, South Africa, suggests metasomatism of a severely melt-depleted substrate by a siliceous, volatile-rich fluid. The fluid reacted with olivine-rich garnet harzburgite, converting olivine to orthopyroxene, forming additional garnet and introducing phlogopite, and small quantities of sulfide and probable carbonate. Extensive reaction (>50%) forming orthopyroxenite resulted from channelized flow in a vein, with orthopyroxene growth in the surrounding matrix from a pervasive grain-boundary fluid. The mineralogy of the reaction assemblage and the bulk composition of the added component dominated by Si and Al, with lesser quantities of K, Na, H, C and S, are consistent with experimental studies of hybridization of siliceous melts or fluids with peridotite. However, low Na, Fe and Ca compared with melts of eclogite suggest a fluid phase that previously evolved by reaction with peridotitic mantle. Garnet and phlogopite trace element compositions indicate a fluid rich in large-ion lithophile (LIL) elements, but poor in high field-strength elements (HFSE), qualitatively consistent with subduction zone melts and fluids. An Os isotope ($T_{RD}$) model age of 2.97 ± 0.04 Ga and lack of compositional zonation in the xenolith indicate an ancient origin, consistent with proposed 2.9 Ga subduction and continental collision in the Kimberley region. The veined sample reflects the silicic end of a spectrum of compositions generated in the Kimberley mantle lithosphere by the metasomatizing effects of fluids derived from oceanic lithosphere. These results provide petrographic and chemical evidence for fluid-mediated Si-, volatile- and trace-element metasomatism of Archean mantle, and support models advocating large-scale modification of regions of Archean subcontinental mantle by subduction processes that occurred in the Archean.

Communicated by J. Hoefs

D. R. Bell (✉) · P. R. Buseck
Department of Geological Sciences and Department of Chemistry/Biochemistry, Arizona State University, 871404, Tempe, AZ 85287-1404, USA
E-mail: David.R.Bell@asu.edu
Fax: +1-480-965-8102

D. R. Bell · T. L. Grove · N. Chatterjee
Department of Earth, Atmospheric and Planetary Sciences, Massachusetts Institute of Technology, Cambridge, MA 02139, USA

M. Grégoire
Observatoire Midi-Pyrénéés, UMR - CNRS 5562, 14 Avenue E. Belin, 31400 Toulouse, France

R. W. Carlson
Department of Terrestrial Magnetism, Carnegie Institution of Washington, 5241 Broad Branch Road N.W., Washington, DC 20015, USA

## Introduction

Ancient continental nuclei, or cratons, are underlain by deep roots of refractory, chemically buoyant peridotite that is depleted in basaltic components such as Na, Ca, Al, and Fe compared with the surrounding mantle (Boyd and McCallister 1976; Boyd and Mertzman 1987). These roots are believed to play a key role in the long-term survival of continental crust, which they isolate from convective instability by a combination of buoyancy and mechanical strength (Jordan 1988, Shapiro et al. 1999).

The important physical properties of Archean lithospheric mantle reflect its unique chemical composition. In addition to the high Mg# [=100 Mg/(Mg+Fe)] typical of Archean cratonic peridotite (Boyd and Mertzman 1987; Griffin et al. 1999; Gaul et al. 2000), many samples, in particular those from the Kaapvaal craton of southern Africa, contain unusually high Si contents (manifested by high modal orthopyroxene) compared with other mantle samples (O'Hara et al. 1975; Boyd 1989; Herzberg 1993). Studies on several other Archean cratons reveal that not all Archean mantle is Si-rich (Kelemen et al. 1998; Kopylova and Russell 2000; Walter 2004), suggesting that this charac-

teristic may be related to specific regional geologic environments in the Archean.

The compositional features of cratonic mantle xenoliths place constraints on the tectonic environment of their formation that are important in the current debate over craton root origins in plumes or subduction environments (e.g., Wyman and Kerrich 2002; Griffin et al. 2003; Parman et al. 2004).

Whereas the high Mg# indicates substantial melt depletion (Boyd 1989), mass balance constraints preclude the simple removal of basalt or komatiite to explain the high $SiO_2$ content of some xenoliths, leading to a variety of other proposals for their origin (Boyd and Mertzman 1987; Kesson and Ringwood 1989; Herzberg 1993; Boyd et al. 1997; Kinzler and Grove 1999; Walter 1998; 1999). Furthermore, experimental studies simulating mantle melting indicate that the Si-rich compositions of xenolith populations from the Kaapvaal, Siberian and Slave cratons are not compatible with residues of melt extraction under the wide range of conditions investigated to date (Walter 2004).

Recently, models emphasizing the importance of melt-rock and fluid-rock interaction in explaining various mantle phenomena, as well as crustal compositions, have achieved increasing prominence (Kelemen 1990, 1995; Kelemen et al. 1993; Niu et al. 1997, Wagner and Grove 1998; Kinzler and Grove 1999). Kesson and Ringwood (1989) proposed a metasomatic solution to the problem of Archean mantle xenolith compositions, in which silicification of occurred in the mantle above a subduction zone by the reaction of olivine with siliceous aqueous fluids to form enstatite. Subsequent variations on this theme (Kelemen et al. 1993, 1998; Rudnick et al. 1994) proposed that the metasomatic agent was a siliceous melt. Such proposals have remained controversial because they require large volumes of metasomatic agent, intruding pervasively on a widespread scale, and because little petrographic evidence for such a process operating in Archean mantle has been presented. Nevertheless, there is evidence of orthopyroxene introduction in xenoliths derived from mantle below the Proterozoic Colorado Plateau (Smith et al. 1999), and of phlogopite and/or enstatite introduction in massif peridotites that are believed to represent mantle wedge environments (Zanetti et al. 1999; Tomoaki et al. 2003). Additionally, several studies of xenoliths from modern subduction-zone environments have implicated metasomatism by volatile-rich, alkaline aluminosilicate melts (MacInnes and Cameron 1994; Schiano et al. 1995; Kepezhinskas et al. 1995, 1996; Prouteau et al. 2001; Laurora et al. 2001).

Pervasive reaction of Archean mantle with fluids or melts is additionally important in its potential implications for the origins of ubiquitous trace element enrichment observed in samples of Archean mantle (Shimizu 1975; Hoal et al. 1994; Pearson et al. 1995) and of diamond and other volatile-rich minerals (Kesson and Ringwood 1989; Bell et al., 2003). Here, we describe the petrographic and chemical features of a sample of Archean mantle that we interpret as evidence for the deposition of silica and other mobile components by reaction of a fluid with refractory mantle harzburgite.

## Sample selection

This study focuses on a veined subcalcic garnet harzburgite nodule from the Boshof Road Dump at Kimberley, South Africa. Material from this diamond mine dump is believed to derive from the Bultfontein kimberlite, in which the sample studied here occurred as a mantle-derived xenolith. This locality is one of few worldwide that produces abundant samples of Archean mantle suitable for textural studies on a large (> 25 cm) scale.

The present work arose from the recent collection of large xenoliths aimed at exploring the significance of textural variations among highly refractory harzburgites in the Bultfontein suite. This collection, which aimed to exclude the products of Mesozoic metasomatism extensively studied previously (e.g., Jones et al. 1982; Kramers et al. 1983; Erlank et al. 1987; Grégoire et al. 2002, 2003), revealed a number of textural variants and texturally heterogeneous samples (Bell et al. 2003). In addition to typical coarse-grained, low-temperature harzburgites, uniformly rich in orthopyroxene, several samples with a heterogeneous spatial distribution of orthopyroxene were encountered. Features of such xenoliths include diffuse veins and irregularly shaped patches of orthopyroxenite, commonly phlogopite-bearing and sometimes with exsolved garnet, within a relatively orthopyroxene-poor matrix. This study concerns the detailed analysis of one such xenolith. Sample BFT137 measures 40×22×15 cm and has the approximate shape of an egg, halved lengthwise. The flat surface is assumed to result from breakage of an originally ovoid xenolith in the plane of a vein of phlogopite-bearing garnet orthopyroxenite. This vein is preserved on the flat sample surface as a selvage some 2–3 cm thick. Preferential fracture of xenoliths along various kinds of veins is commonly observed at Kimberley. The remainder of the xenolith consists of clinopyroxene-free garnet harzburgite, with sparsely distributed phlogopite.

Contrasting with such samples are uniformly orthopyroxene-poor, olivine-rich harzburgite containing sparse subcalcic garnet and relatively abundant discrete (i.e., non-symplectic) magnesiochromite. One example of this group (BFT147) was studied for comparison with the veined sample. This xenolith measures ~20×10×10 cm and is a homogeneous, orthopyroxene-poor garnet harzburgite/dunite with accessory chromite and large patches of coarse phlogopite.

## Analytical methods

Sample BFT137 was sectioned in a plane perpendicular to the orthopyroxenite vein, and perpendicular to the long axis of the xenolith, and four large (5×7.5 cm) polished thin sections were prepared from the slab

shown in Fig. 1. A single large thin section of sample BFT147 was prepared. The thin sections were mapped chemically on a 10-μm-grid scale for Mg, Al, and Ca using the JEOL733 electron microprobe at MIT and the maps analyzed spatially with commercial image processing software. Full major element chemical analyses of each mineral, including traverses perpendicular to the vein and core-rim were performed on the JEOL JXA-8900 electron probe at the Geophysical Laboratory, Carnegie Inst. of Washington. The electron microprobe analyses were designed to provide high levels of precision for individual point analyses. Counting times for major elements (i.e., > 10 wt.% oxide) were typically set to yield < 0.2% relative precision based upon counting statistics. All minerals were analyzed at 15 kV accelerating potential, with the following beam currents measured on the Faraday cup: 40 ± 2 nA (orthopyroxene), 60 ± 2 nA (garnet), 150 ± 2 nA (olivine, phlogopite). Extended counting times up to 180 s on peak and background were used for trace elements.

A wider range of trace elements was determined in situ on selected grains in > 120-mm-thick polished sections by LA-ICP-MS at the University of Cape Town. The Perkin Elmer Elan 6000 ICPMS instrument was coupled to a Cetac LSX-200 laser ablation module that uses a 266-nm frequency-quadrupled Nd-YAG laser. Details of the LA-ICP-MS analytical procedure appear in Grégoire et al.(2002). Bulk compositions for vein and substrate were computed by combining modal proportions from the chemical maps with electron microprobe and LA-ICP-MS mineral analyses.

Bulk analyses of Re and Os concentration and isotope composition of BFT137 were determined on a sample of the matrix immediately adjacent to the vein, extending 5 cm into the matrix from the vein boundary. The analyses were performed at the Carnegie Institution of Washington, Department of Terrestrial Magnetism using techniques described by Carlson et al. (1999).

## Mineralogy and texture

A macroscopic view of the sample is given in Fig. 1, illustrating the linear selvage (vein) of coarse-grained orthopyroxenite bounding a matrix of coarse-grained harzburgite. The boundary of the vein is not sharp, but appears to grade over a distance of one to two centimeters, giving rise to a somewhat indistinct boundary in thin section. Modal heterogeneities in other Bultfontein harzburgite samples have a similarly diffuse character. The modal compositions of the vein and host matrix are given in Table 1.

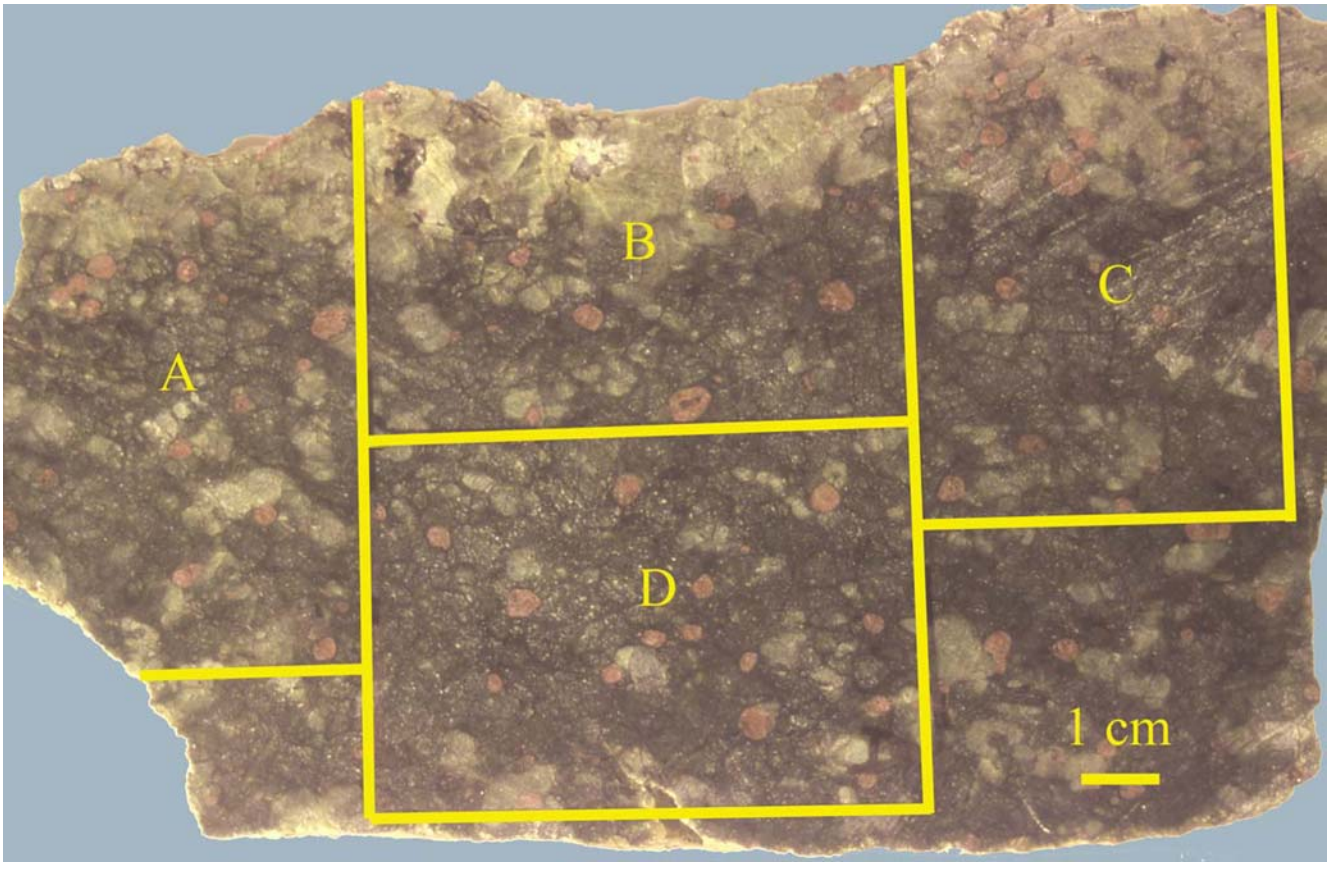


**Fig. 1** 1-cm-thick slab of sample BFT137, cut at right angles to the vein and the long axis of the xenolith. Orthopyroxene-rich vein occurs along the top edge of sample and the position of four large thin sections, A, B, C and D, used for mineral analyses and bulk compositional calculations is illustrated

**Table 1** Modal compositions (volume%)

| Mineral | Volume% | | |
|---|---|---|---|
| | BFT137 Vein | BFT137 Host matrix | BFT147 |
| Olivine | 29.7 | 77.9 | 88.0 |
| Enstatite | 56.6 | 18.2 | 4.5 |
| Garnet | 6.5 | 3.6 | 2.5 |
| Cr-spinel | – | – | 2.5 |
| Phlogopite | 6.7 | – | 2.4 |
| Carbonate* | 0.3 | 0.3 | – |
| Sulfide | 0.3 | – | – |

*Carbonate inferred from serpentine-brucite-calcite assemblages with primary grain outlines, described in text. The carbonate abundances inferred from these pseudomorphs were determined over the entire xenolith and therefore reported here as equal in vein and matrix

## Vein

Besides modally dominant enstatite, the vein region also contains garnet, subordinate olivine, abundant coarse phlogopite, and large (up to 0.5 mm diameter) subspherical to euhedral sulfide grains. Occasional patches with the outline of a primary mineral (Figs. 2a, 2b) but comprising a fine-grained intergrowth dominated by serpentine are inferred to be pseudomorphs after a carbonate, as described by Berg (1986). Orthopyroxene grains are mostly equant without preferred orientation and olivine occurs interstitially and as inclusions to the orthopyroxene. Most garnet grains are rounded, with occasional irregular to poikilitic grain shapes (Fig. 3). The primary minerals in both vein and host matrix are also affected to various degrees by hydrothermal

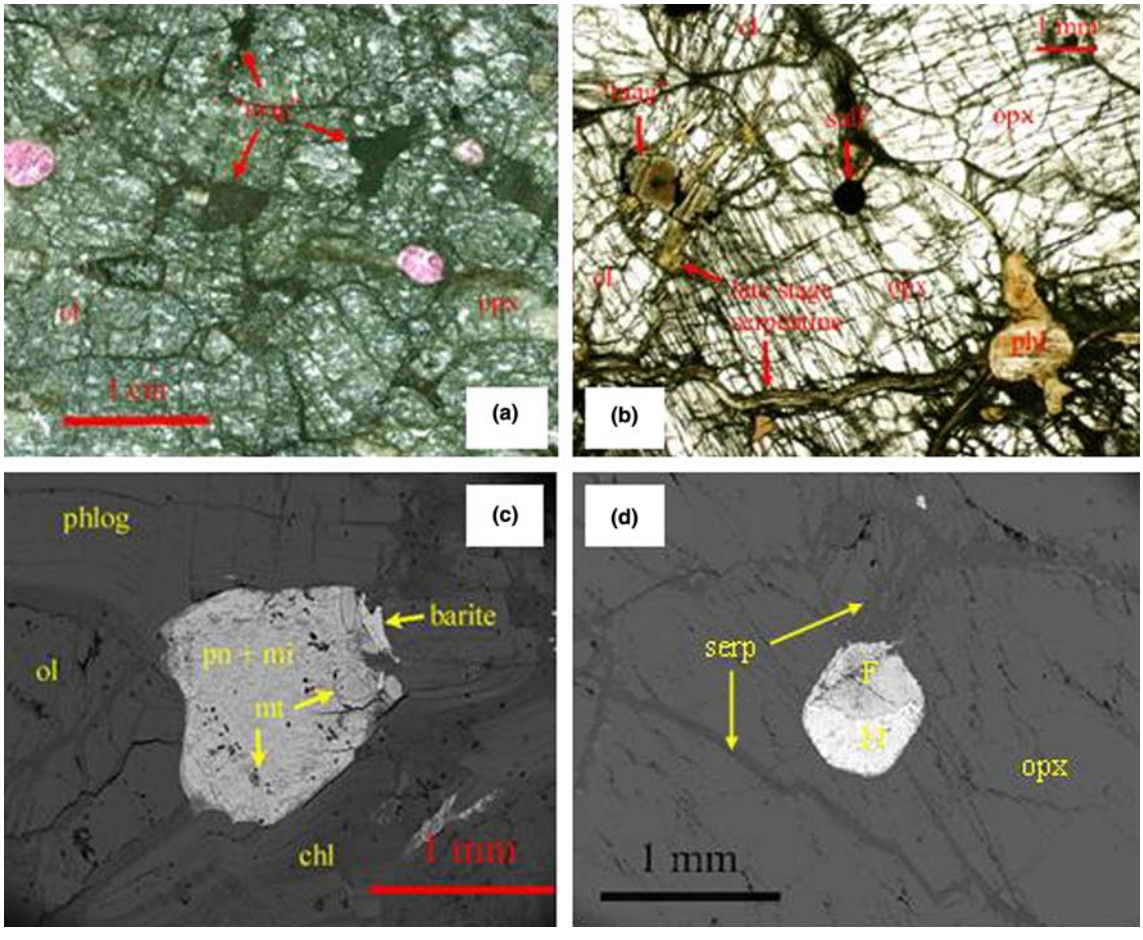


**Fig. 2** Petrographic features of sample BFT137. **a** Low-magnification view of sawn slab surface, illustrating primary-appearing outlines of serpentine-brucite pseudomorphs (mag) after probable carbonate (Berg 1986). **b** Thin section plane-polarized light view of vein assemblage, including phlogopite (phl), enstatite (opx), olivine (ol), serpentine-brucite pseudomorphs (''mag''), sulfides (sulf) and veins of serpentine formed during emplacement-related hydrothermal alteration. **c** Backscattered electron image of vein assemblage. Sulfide surrounded by olivine (ol) and by phlogopite (phl) partially altered along cleavage planes (chl). The original sulfide is recrystallised to an Fe-oxide (mt) and Ni-rich secondary sulfides (pn-mi), with secondary barite formed along one margin of the grain. **d** Secondary Ni-sulfide (N) and Fe-oxide (F) assemblages in a pseudomorph after original euhedral sulfide crystal. The oxide portion of the assemblage is located where a prominent serpentine vein (serp) that transgresses the enclosing enstatite (opx) intersects the original sulfide

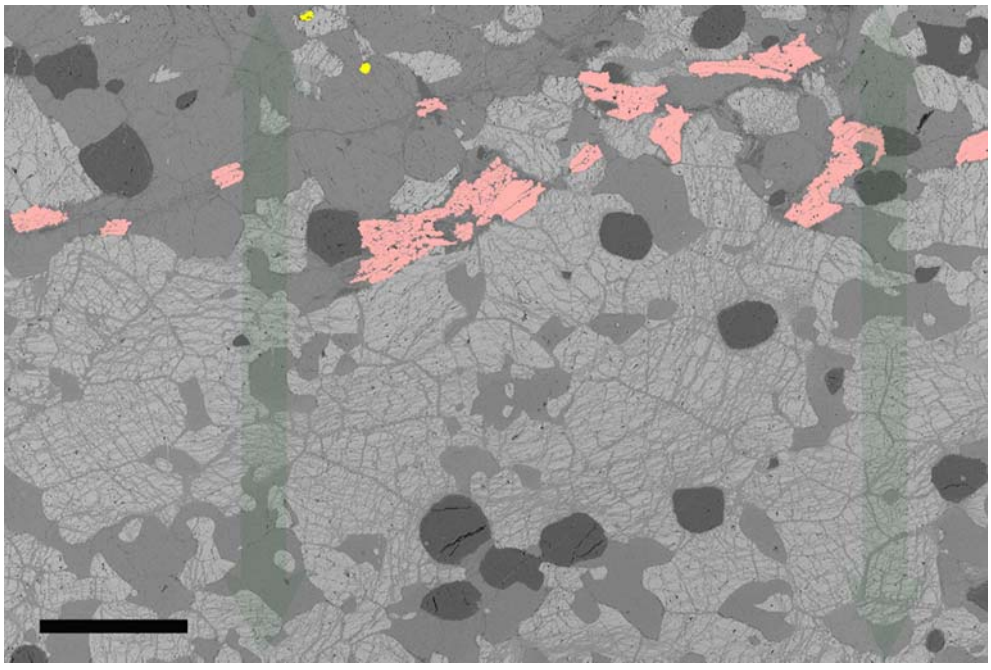

**Fig. 3** Magnesium map of a portion of BFT137, section B (Fig. 1), determined by WDS analysis. The *gray scale*is proportional to Mg concentration. *Light grey*– olivine, *medium gray*– orthopyroxene, *dark grey round grains*– garnets. Phlogopite has been colored pink and sulfide yellow. The orthopyroxene-rich vein with phlogopite occurs in the upper portion of the section. Orthopyroxene exhibits amoeboid to sinuous habit, with olivine inclusions. The position of the compositional traverses (Fig. 4) marked by *broad arrows*. Scale bar = 1 cm

processes inferred to be associated with kimberlite emplacement. Olivine is partially replaced (10–20%) by a network of chrysotile. Most sulfide grains are extensively oxidized, comprising a mixture of Ni-rich sulfides, magnetite, and fine-grained silicate, occasionally with associated barite (Fig. 2c). This alteration can in some cases be traced directly to individual veins of serpentine (Fig. 2d) and is common in mantle-derived sulfides (Lorand 1993). Phlogopite contains cleavage-parallel zones of chloritization, apparent as low-atomic number regions in backscattered electron images (Fig. 2c).

### Host matrix

The host region consists of the same minerals, except for sulfide, but with more olivine and less enstatite, garnet, and phlogopite. Carbonate pseudomorphs also occur in the matrix, but are more difficult to quantify unambiguously than the other phases as a result of serpentinization. Phlogopite in the host is only present in a single large, elongated patch running oblique to the main orthopyroxenite vein. This region of the matrix is locally richer in enstatite and appears to be a poorly defined, vein-like structure. Garnets are distributed evenly in the matrix and are rounded to subrounded.

The color-coded Mg map (Fig. 3) highlights the texture of orthopyroxene in the matrix. Orthopyroxenes are commonly highly irregular in outline, containing numerous embayments, and commonly completely enclosing olivine grains. Many orthopyroxene grains are elongate and sinuous, appearing to indicate original growth along grain boundaries, followed by poikilitic engulfment of olivine as the grains grew. Because enstatite growth requires introduction of silica, the texture suggests growth from a dispersed, grain-boundary medium. Orthopyroxene shapes in the vein are not as sinuous, but there are many instances of rounded olivine inclusions, suggesting that the enstatite vein also grew by reaction and replacement of olivine. The greater orthopyroxene abundance in the vein results in the mutual interference of grains, and their more equant habit suggests that growth by reaction proceeded to a more advanced stage, reflecting extended reaction progress in a region of greater reactant supply. These modal abundances and internal textures of the vein suggest a region of channelized fluid flow. However, the fluid conduit could have been significantly narrower than the vein itself, and its original dimensions or form are not evident.

In contrast to BFT137, BFT147 has much less garnet (2.5%) and enstatite (4.5%) and no carbonate pseudomorphs. However, it contains about 2% magnesiochromite. Large phlogopite patches (2%) are present. Enstatite also has a habit suggesting growth from an inter-granular medium, but the grains are small and appear to represent the initial stages of such a process.

## Mineral compositions

### Major elements

Average mineral compositions determined by electron microprobe are given in Tables 2 and 3. Garnet, orthopyroxene and olivine are internally homogeneous except for small variations (up to 0.4 wt.%) in CaO and $Cr_2O_3$ in garnet. A consistent difference of 0.1–0.2 wt.% exists between cores and rims, with zoning to higher CaO and lower $Cr_2O_3$ in the outermost 300 micrometers. This zonation may result from the infiltration of small quantities of kimberlite-derived fluids at, or shortly before, eruption. Variations in the CaO and

**Table 2** Major and trace element compositions (wt.%) for primary minerals in BFT137, determined by electron microprobe*

| | Olivine n = 66 | Enstatite n = 96 | Garnet n = 104 | Phlogopite n = 16 |
|---|---|---|---|---|
| $SiO_2$ | 41.8 (2) | 58.2 (3) | 42.5 (3) | 41.7 (5) |
| $TiO_2$ | < 0.005 | < 0.01 | 0.023 (7) | 0.089 (5) |
| $Al_2O_3$ | < 0.005 | 0.88 (1) | 20.6 (1) | 12.9 (2) |
| $Cr_2O_3$ | 0.038 (4) | 0.48 (2) | 5.36 (10) | 1.06 (2) |
| FeO | 6.06 (4) | 3.62 (4) | 5.67 (6) | 2.25 (3) |
| MnO | 0.080 (6) | 0.088 (9) | 0.29 (1) | 0.017 (4) |
| MgO | 52.8 (3) | 36.5 (2) | 23.2 (2) | 26.5 (3) |
| CaO | 0.016 (3) | 0.35 (2) | 3.28 (16) | < 0.01 |
| $Na_2O$ | 0.013 (4) | 0.18 (1) | 0.03 (2) | 0.11 (3) |
| $K_2O$ | n.a. | n.a. | n.a. | 10.1 (3) |
| NiO | 0.386 (6) | 0.10 (1) | n.a. | 0.208 (7) |
| $P_2O_5$ | 0.009 (4) | n.a. | 0.053 (8) | n.a. |
| F | n.a. | n.a. | n.a. | 0.24 (5) |
| Cl | n.a. | n.a. | n.a. | 0.075 (5) |
| BaO | n.a. | n.a. | n.a. | 0.07 (2) |
| $Rb_2O$ | n.a. | n.a. | n.a. | 0.014 (6) |
| Mg# | 93.95 (4) | 94.73 (5) | 87.92 (14) | 95.46 (9) |
| Cr# | 26.6 (9) | 14.8 | (3) | 5.23 (9) |

* Mean and standard deviation (last significant digits) of all analyses (n = number of analyses). n.a. not analyzed. Data for phlogopite are derived only from areas that appear fresh in BSE imaging (see text). Analyses of altered phlogopite areas are excluded

**Table 3** Major and trace element compositions (wt.%) for primary minerals in BFT147, determined by electron microprobe

| | Olivine | Opx | Garnet | Phlogopite | Spinel |
|---|---|---|---|---|---|
| $SiO_2$ | 40.5 | 58.2 | 41.3 | 42.0 | 0.07 |
| $TiO_2$ | < 0.005 | 0.009 | 0.025 | 0.11 | 0.11 |
| $Al_2O_3$ | 0.008 | 0.78 | 18.8 | 12.9 | 8.70 |
| $Cr_2O_3$ | 0.039 | 0.59 | 7.49 | 1.50 | 60.8 |
| FeO* | 5.82 | 3.47 | 5.6 | 2.48 | 15.0 |
| MnO | 0.092 | 0.093 | 0.30 | 0.021 | 0.25 |
| MgO | 52.6 | 37.2 | 22.6 | 26.0 | 14.1 |
| CaO | 0.027 | 0.31 | 3.18 | < 0.03 | < 0.03 |
| $Na_2O$ | 0.018 | 0.16 | 0.03 | 0.09 | < 0.03 |
| $K_2O$ | n.a. | n.a. | n.a. | 9.71 | n.a. |
| NiO | 0.353 | 0.092 | 0.004 | 0.21 | 0.10 |
| $P_2O_5$ | n.a. | n.a. | 0.07 | n.a. | n.a. |
| Cl | n.a. | n.a. | n.a. | 0.55 | n.a. |
| F | n.a. | n.a. | n.a. | 0.17 | n.a. |
| BaO | n.a. | n.a. | n.a. | 0.11 | n.a. |
| Mg# | 94.1 | 95.0 | 87.8 | 94.7 | 62.6 |
| Cr# | 33.7 | 21.1 | 7.2 | 82.4 | |

FeO*: all Fe reported as FeO. n.a. = not analyzed

$Cr_2O_3$ content of grain cores also exceed analytical uncertainty, but do not vary systematically across the xenolith. Phlogopite is homogeneous in its major components, but certain trace elements show variations that exceed analytical uncertainties. All minerals are extremely magnesian, with olivine Fo94.0, orthopyroxene En94.7, phlogopite Mg# = 95.5 and garnet Mg# = 87.9. The garnet contains 5.4 wt.% $Cr_2O_3$ and 3.3 wt.% CaO and thus falls well within the G10 (“harzburgitic”) field defined by Dawson and Stephens (1975) and Gurney (1984). All phases are extremely low in $TiO_2$. The orthopyroxene contains an unusually high concentration of Na (0.17 wt.% $Na_2O$) for this low Ti content. Thermobarometry calculations based upon Fe–Mg exchange between coexisting garnet and olivine (O’Neill and Wood 1979; O’Neill 1980) and Al content of orthopyroxene in equilibrium with garnet (Brey and Köhler 1990) give equilibration conditions of 3.6 GPa and 1000°C.

Analytical traverses perpendicular to the vein in BFT137 reveal that compositions are equilibrated across the xenolith, with no compositional differences between minerals in vein and matrix (Fig. 4). The decimeter-scale homogeneity confirms inferences from chemical compositions that vein formation is ancient and not related to metasomatism shortly before eruption.

The minerals in BFT147 (Table 3) are also highly magnesian, the olivine (Fo94.1) and enstatite (En95.0) marginally more so than in BFT137. Ni in BFT147 olivine (0.353 wt.% NiO) is lower than in the olivine of BFT137 (0.386 wt.% NiO). Relatively low Ni content is a general feature of olivines from the Kimberley orthopyroxene-poor harzburgites (Bell et al. 2003). Garnet has somewhat higher Cr (7.5 wt.% $Cr_2O_3$) and lower Ca (3.2 wt.% CaO) content than BFT137. The spinel is Cr-rich (61 wt.% $Cr_2O_3$). Phlogopite is richer in K and Cl

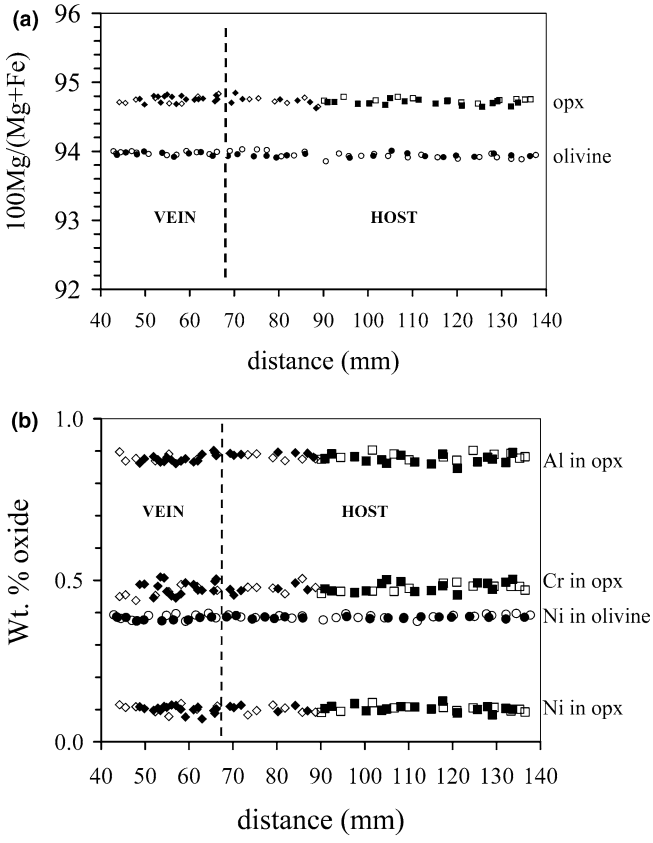


**Fig. 4 a**, **b** Electron microprobe traverses across the xenolith illustrating compositional homogeneity. The two parallel traverses (one represented by open symbols, the other by solid symbols) were determined on Sect. B (diamond symbols), continuing onto Sect. D (squares). See Figs. 1 and 3 for location of the traverses

than the phlogopite in BFT137. The garnet and spinel exhibit minor variations in Cr content from grain to grain, but no core to rim zonation was noted. This sample equilibrated at 3.4 GPa and 940°C, within uncertainty of the conditions calculated for BFT137.

## Trace elements

Average LA-ICP-MS analyses for minerals in BFT137 are reported in Table 4. The garnets in BFT137 are homogeneous from grain to grain, and in spots analyzed at garnet cores and rims (Fig. 5). The garnet chondrite-normalized REE patterns are broadly similar to those determined for garnets from low-temperature harzburgites on the Kaapvaal Craton (Shimizu 1975; Hoal et al., 1994; Grégoire et al., 2003) but are notable in having HREE concentrations at the low end, and LREE concentrations at the high end, of the range for Kimberley samples. The BFT137 garnet patterns differ from the sinusoidal patterns skewed towards LREE enrichment that have been observed in many subcalcic Cr-pyrope inclusions in diamond (Shimizu and Richardson 1987; Stachel et al. 2004), some diamondiferous peridotites (Pokhilenko et al. 1993, Stachel et al. 1998; Shimizu et al. 1999), and sample BFT147 in this study

**Table 4** Mineral trace element compositions (wt. ppm) determined by LA-ICP-MS

| Sample | Garnet BFT137 n = 7 | Olivine BFT137 n = 2 | Enstatite BFT137 n= 2 | Phlogopite BFT137 n = 3 | Garnet BFT147 n = 2 |
|---|---|---|---|---|---|
| Sc | 99 (17) | 1.9 (9) | 2.7 (13) | 2.7 (9) | 88 (3) |
| V | 172 (24) | 5.9 (2) | 38 (14) | 86 (13) | 170 (11) |
| Ni | 37 (4) | 2313 (157) | 550 (177) | 969 (93) | 29 (1) |
| Co | 31 (4) | 91 (6) | 34 (11) | 31 (4) | 30 (1) |
| Ga | n.d. | n.a. | n.a. | 9 (2) | 0.86 (10) |
| Rb | n.a. | n.a. | n.a. | 161 (25) | n.a. |
| Sr | 0.40 (5) | 0.68 (8) | 2.3 (6) | 8.2 (32) | 1.19 (7) |
| Ba | n.a. | n.a. | n.a. | 527 (195) | n.a. |
| Y | 1.8 (6) | n.d. | n.d. | 0.03 (1) | 1.53 (6) |
| U | 0.054 (23) | n.a. | n.a. | n.a. | 0.073 (16) |
| Ti | 107 (17) | 4.8 (7) | 24 (5) | 283 (55) | 66 (2) |
| Zr | 42 (10) | 0.19 (9) | 0.52 (15) | 3.2 (8) | 22 (1) |
| Hf | 0.76 (16) | n.a. | n.a. | n.a. | 0.46 (2) |
| Nb | 0.13 (4) | 0.15 (0.1) | 0.20 (11) | 11 (2) | 0.28 (4) |
| Pb | n.a. | n.a. | n.a. | 1.17 (5) | n.a. |
| La | 0.14 (1) | | | | 0.15 (7) |
| Ce | 0.38 (8) | | | | 1.53 (12) |
| Pr | 0.20 (4) | | | | 0.84 (8) |
| Nd | 2.64 (30) | | | | 8.60 (57) |
| Sm | 1.86 (25) | | | | 1.47 (1) |
| Eu | 0.70 (10) | | | | 0.33 (4) |
| Gd | 1.78 (36) | | | | 0.71 (3) |
| Dy | 0.62 (17) | | | | 0.33 (5) |
| Ho | 0.074 (20) | | | | 0.044 (7) |
| Er | 0.11 (3) | | | | 0.11 (2) |
| Yb | 0.11 (3) | | | | 0.11 (2) |
| Lu | 0.021 (5) | | | | 0.023 |

Mean and standard deviation (in last significant digit) of *n* analyses. *n.d.* not detected, *n.a.* not analyzed

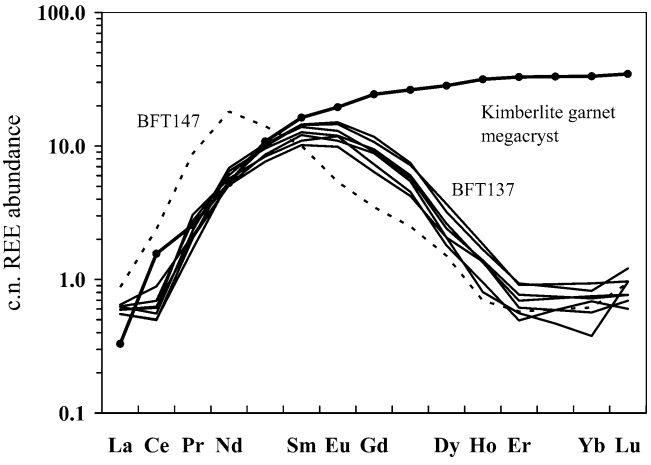


**Fig. 5** Chondrite-normalized REE abundances in BFT137 garnets and a sible analysis from BFT147, determined by LA-ICP-MS. The REE pattern of a garnet megacryst from kimberlite (D. Bell and A. Kennedy unpubl. SIMS analysis) is shown for comparison. Chondrite abundances are from Anders and Grevesse 1989

(Fig. 5). In contrast to these, the REE pattern in BFT137 approximates a symmetric bell-shape, i.e., MREE enriched ~10X over LREE and HREE (Fig. 5). The typical diamond-inclusion-type patterns (and BFT147) show a peak in normalized REE abundances at Nd, whereas those in the present sample show a peak at Sm to Eu. A similar pattern to BFT137, but with somewhat higher HREE content, is reported by Stachel et al. (1999) in a harzburgitic diamond inclusion garnet from Mwadui, Tanzania.

The very low Ti concentration in the BFT137 garnet results in a marked anomaly in the mantle-normalized trace element diagram (Fig. 6), where the elements are plotted in terms of increasing compatibility during basalt petrogenesis. However, Zr, Hf, and Nb abundances are not unusually low in concentration compared with neighboring REE. They are, however, a factor of 2 to 4 lower than the abundances in a garnet from a sheared peridotite, and the $(La/Nb)_N$, $(Sm/Zr)_N$, $(Sm/Hf)_N$ and $(Gd/Ti)_N$ are all substantially higher than for the sheared peridotite example (Fig. 6). The sheared peridotite is considered to result from the metasomatic effects of a silicate melt related to the Cr-poor megacryst suite and to kimberlite (Gurney and Harte 1980; Hops et al.1989). These ratios indicate relative high field-strength element (HFSE) depletion of the BFT137 garnet in relation to garnets equilibrated with the kimberlite-related megacryst parent magma, which has LIL-element to HFSE ratios similar to OIB. The garnet in BFT147 has approximately half the Ti, Zr, and Hf concentrations of the BFT137 garnet, and approximately twice the U, Nb and Sr concentrations. Other transition element concentrations of the garnets in the two samples are similar.

Phlogopites in BFT137 show greater compositional variability than the garnets, probably as a result of secondary alteration. Back-scattered electron imaging of

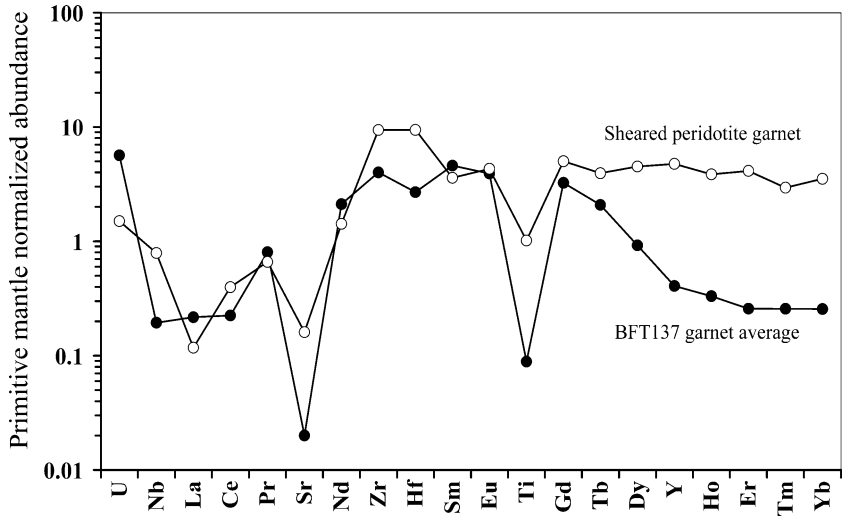


**Fig. 6** Primitive mantle-normalized trace elements diagram comparing the average BFT137 garnet with the trace element pattern of a garnet from the sheared garnet lherzolite PR89-1 from the Premier kimberlite (Grégoire et al. 2003). Notable differences include lower Nb, Zr, Hf, Ti, Sr and HREE in BFT137, but similar LREE abundances. Primitive mantle abundances are from McDonough and Sun (1995)

phlogopite accompanied by trace element electron microprobe analysis reveals zones from which the alkalis and alkaline-earth elements have been leached. These may be a cause of the substantial heterogeneity in Ba analyses of phlogopite by LA-ICP-MS (Table 4). Electron microprobe analyses are less variable than the ICP-MS analyses, presumably because of the higher spatial resolution and greater care (backscattered electron imaging) with which analytical areas may be selected, hence avoiding areas of alteration. Phlogopite in BFT137 contains an average of approximately 150 ppm Rb and 550 ppm Ba. The Rb content is lower than that of all metasomatic micas analyzed by Grégoire et al. (2002) using the same analytical procedures, and the Ba content is higher than all but one sample. The $TiO_2$ content of the BFT137 phlogopite (0.09 wt.%) is distinctly lower than that of micas in metasomatic xenoliths and at the low end of primary micas in garnet peridotites. Nb, Zr, and Pb contents are not distinguishable from metasomatic phlogopite in micaceous xenoliths (Grégoire et al. 2002). The phlogopite of BFT147 is also poor in $TiO_2$ (0.12 wt.%) and contains notably higher Cl concentration (0.55 wt.%) than that of BFT137 (0.08 wt.%).

**Table 5** Calculated bulk compositions (wt.%) [a]

| | BFT137 Vein | BFT137 Host | BFT147 | BFT147 Phl-FREE[b] |
|---|---|---|---|---|
| $SiO_2$ | 50.6 | 44.5 | 40.3 | 40.3 |
| $TiO_2$ | 0.011 | 0.002 | 0.006 | 0.004 |
| $Al_2O_3$ | 2.68 | 0.90 | 1.06 | 0.76 |
| $Cr_2O_3$ | 0.69 | 0.30 | 1.90 | 1.87 |
| FeO | 4.39 | 5.61 | 5.84 | 5.91 |
| MnO | 0.094 | 0.089 | 0.098 | 0.100 |
| MgO | 39.8 | 48.8 | 49.5 | 50.1 |
| CaO | 0.41 | 0.19 | 0.12 | 0.12 |
| $Na_2O$ | 0.11 | 0.033 | 0.026 | 0.024 |
| $K_2O$ | 0.66 | < 0.01 | 0.23 | < 0.01 |
| NiO | 0.19 | 0.32 | 0.32 | 0.33 |
| $P_2O_5$ | 0.006 | 0.009 | n.a. | n.a. |
| $H_2O$[c] | 0.26 | < 0.01 | 0.095 | < 0.01 |
| S[d] | 0.12 | < 0.01 | < 0.01 | < 0.01 |

[a] Calculated from mineral analyses and element-map-based modal analysis
[b] Analysis recalculated on phlogopite-free basis
[c] $H_2O$ calculated assuming 4 wt.% $H_2O$ in phlogopite, none in other minerals
[d] S calculated assuming 35 wt.% S in sulfide, none in other minerals

## Whole-rock compositions

The bulk compositions of the vein and matrix in BFT137 and of the orthopyroxene-poor sample BFT147 were computed by combining the modal proportions and mineral compositions, and are reported in Table 5. The vein is richer in $SiO_2$, $Al_2O_3$, $Cr_2O_3$, CaO, $Na_2O$, $K_2O$, $H_2O$ and S, and poorer in FeO, MgO and NiO than the matrix. BFT147 has a composition similar to the matrix of BFT137, but is richer in $Cr_2O_3$ and poorer in $SiO_2$. Also listed in Table 5 is the composition of BFT147 recalculated on a $K_2O$- and $H_2O$-free basis, proposed as a possible pre-metasomatic protolith composition for this sample. Aspects of the major element compositions are plotted in Fig 7, where they are compared with the Kaapvaal data of Boyd and coworkers. Fig. 7a illustrates the highly Si-rich character of the vein, the relatively Si-poor character of the BFT137 matrix, and the exceptionally Si-poor and Mg-rich character of the orthopyroxene-poor sample BFT147. The range of compositions determined for four sections of the matrix of BFT137 spans approximately the full range of Mg/Si ratios for a given olivine Mg# in Kaapvaal low-temperature peridotites, and demonstrates that local modal variations can be responsible for much of the scatter seen in such plots, as noted by Boyd and Mertzman (1987). In contrast, the variation in Ca and Al contents (like that of Mg#) accounts for only a small percentage of the variability in the regional data set (Fig. 7b).

If the serpentine-brucite patches, which we interpret as carbonate pseudomorphs, were composed of original magnesite (the likely stable carbonate under these P-T-X

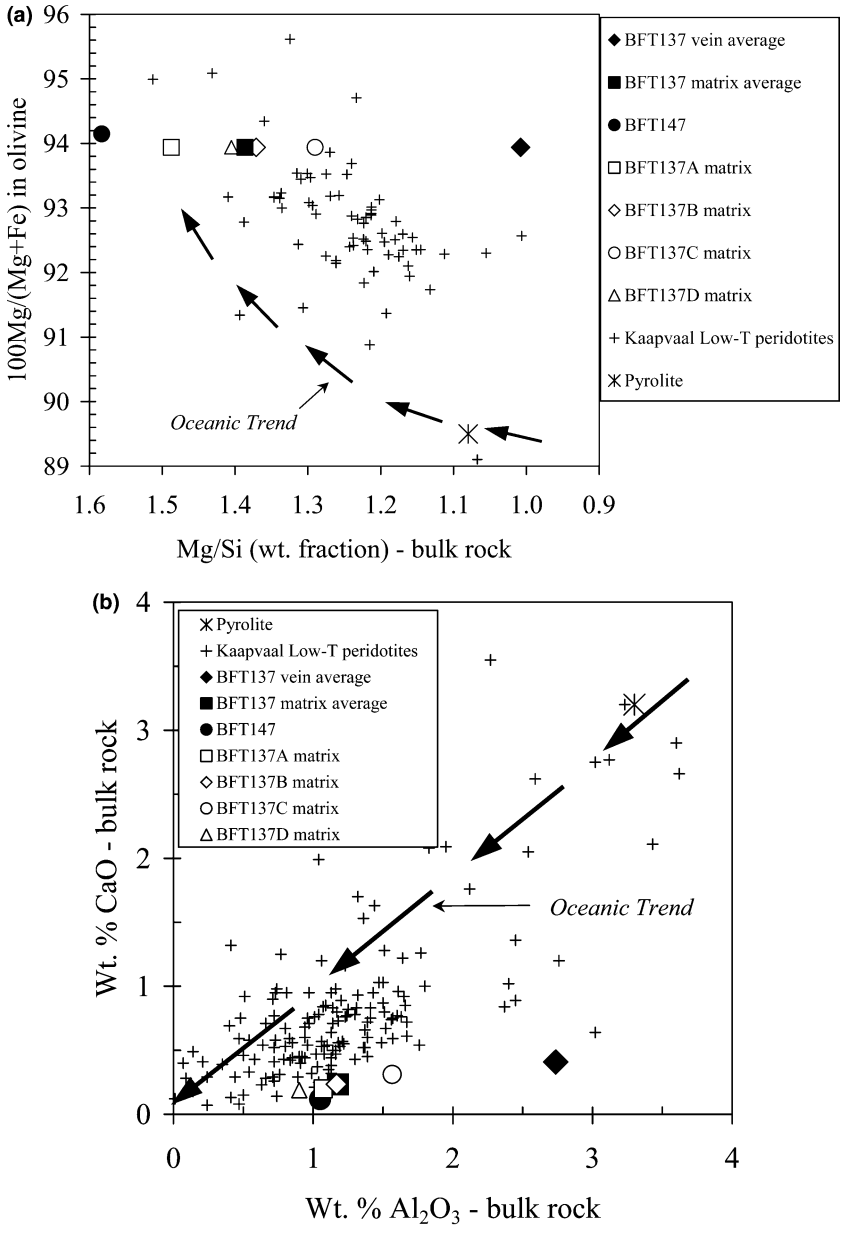


**Fig. 7** **a** Fo content of olivine vs Mg/Si of bulk rock and **b** CaO vs. $Al_2O_3$ for BFT137 components (the four large thin sections illustrated in Fig. 1, and average vein and matrix concentrations) and Kaapvaal low-temperature peridotite whole rock analyses compiled from the literature. The *arrows* represent the trend defined by average compositions of oceanic peridotite suites (Boyd 1989)

conditions), then BFT137 would have contained approximately 0.15 wt.% $CO_2$.

## Re–Os isotopes

The Re–Os abundances and isotope compositions are presented in Table 6. The Re and Os concentrations are typical of Kaapvaal peridotites. The Re abundance of 0.116 ppb is close to the average Kaapvaal peridotite, but is higher than most harzburgites from Kimberley (average 0.031 ppb; Carlson and Moore 2004). The low γOs of −16.3 is typical of Archean subcontinental mantle and indicates a long time-integrated history of extreme Re-depletion, consistent with Archean melt extraction. The Re-depletion age ($T_{RD}$) of 2.97 ± 0.04 Ga is among the oldest recorded for Kimberley samples (Walker et al. 1989; Pearson et al. 1995a; Carlson et al. 1999; Simon et al. 2003a, b). However, the depleted mantle model age ($T_{MA}$) > 4.5 Ga indicates late-stage Re addition, probably during emplacement-

**Table 6** Re–Os isotope data for BFT137

| | |
|---|---|
| Re | 0.116 ppb |
| Os | 2.714 ppb |
| $^{187}Re/^{188}Os$ | 0.2045 ± 0.0016 |
| $^{187}Os/^{188}Os$ | 0.10753 ± 0.00027 |
| $^{187}Os/^{188}Os_{90}$ | 0.10722 ± |
| $\gamma Os_{90}$ | −16.3 ± 0.3 |
| $T_{RD}$ | 2.97 ± 0.04 |
| $T_{MA}$ | 5.52 ± 0.11 |

related hydrothermal serpentinization that resulted in sulfide recrystallisation.

## Discussion

### Textural evidence for metasomatic introduction of orthopyroxene

The petrographic features of enstatite, including its distribution and grain shapes, are evidence that this mineral grew from a grain-boundary fluid that permeated the xenolith, with a greater fluid supply and degree of reaction in the vein. Similar evidence has been presented for fluid-mediated orthopyroxene growth in mantle-derived xenoliths from the Colorado Plateau (Smith et al.1999; Smith 2000) and the southwestern Pacific (McInnes and Cameron 1994). Both these suites of samples derive from the mantle in the neighborhood of subduction zones, which are thought to be the source of the metasomatizing fluids (Smith et al. 2000, 2004; McInnes and Cameron 1994; McInnes et al. 2001). The orthopyroxenes from the Colorado Plateau xenoliths are richer in small olivine inclusions than the Bultfontein sample, and also are characterized by a particular Al-poor composition. In contrast, the Bultfontein orthopyroxene compositions are typical for low-temperature cratonic peridotites and reflect equilibrium with an aluminous phase (garnet or spinel). These textural and chemical differences are not surprising given the probability that the vein under discussion is likely to be much older (~2.9 Ga) than the Cenozoic to recent age for the other examples. Partial textural re-equilibration during this time may have removed small inclusions and promoted chemical equilibration with other minerals in the surrounding mantle. Chemical equilibration with garnet or spinel would have removed any evidence that the orthopyroxene in BFT137 was originally low in Al. The xenolith reveals that chemical equilibrium has been achieved on a length scale of at least a decimeter, and may extend further.

In sample BFT137, the enstatite in the vein is accompanied by volatile-rich phases, including phlogopite, sulfide and probable carbonate. The sulfide is confined to the vein, whereas carbonate and phlogopite occur both in matrix and vein. Phlogopite is less abundant in the matrix, but the inferred carbonate pseudomorphs occur in similar proportions in both. Observations of other veined, orthopyroxene-rich samples reveal that these pseudomorphs are sometimes concentrated in a zone outside of the vein defined by modal enstatite. The distribution of pseudomorphs suggests that carbon, in contrast to sulfur, is relatively mobile during fluid-peridotite reaction.

The abundances of phlogopite and enstatite are correlated. In addition, the higher modal abundance of garnet in the vein requires introduction of Al. However, garnet grain shapes appear similar in vein and matrix, and distinctive textural evidence for metasomatic garnet growth is lacking. There is also no evidence that garnet exsolved from aluminous enstatite, as inferred for some other samples of Kaapvaal craton peridotite (Cox et al. 1987; Canil 1991; Saltzer et al. 2001; Lahaye and Brey 2003; Dawson 2004). The preservation of orthopyroxene textures and lack of evidence for garnet exsolution suggest that metasomatic reaction occurred at temperatures not substantially above those recorded by the xenolith (~1000°C) at the time it was sampled by the rising kimberlite magma.

The conclusion that enstatite was introduced into this xenolith by a mobile phase has important consequences for models of cratonic mantle evolution. The Si-rich nature of Archean low-temperature peridotite from the Kaapvaal craton mantle root has been long-recognized and its origins much debated (O'Hara et al. 1975; Herzberg 1993; Walter 2004). Although metasomatic models have played an important role in this debate (Kesson and Ringwood 1989; Rudnick et al. 1994; Kelemen et al. 1998), the present description represents, to our knowledge, the first report of petrographic evidence in support of such a process in the Kaapvaal mantle. Evidence from sample BFT137 indicates that introduction of phlogopite, some garnet, and trace amounts of sulfide and carbonate accompanies enstatite formation, whereas olivine, and possibly Cr-spinel are removed in the process.

In sample BFT147, which contains only 4.5% enstatite, the textures also suggest metasomatic introduction. Although enstatite distribution is not confined to veins or patches, grains appear to be aligned in linear arrays parallel to their individual direction of elongation. The initial stages of enstatite growth are represented by small, sinuous orthopyroxenes, very different in habit from the equant, cm-sized crystals that typify Si-rich cratonic peridotite. The sample also contains metasomatic phlogopite. These minerals may represent the initial stages of infiltration by a volatile-rich fluid, in which fluid-rock interaction has been insufficient for significant quantities of enstatite growth, or where the composition of the fluid was richer in K and poorer in Si as a result of chromatographic fractionation during its passage through, and reaction with, the mantle (Navon and Stolper 1987). In our model, the phlogopite-bearing, but orthopyroxene-poor assemblages are proposed to occur distal to zones of concentrated fluid flow, and should bear additional features of metasomatism by extensively fractionated fluids (e.g., Bodinier et al. 2004). Indeed, the trace element composition of BFT147 phlogopite and garnet reflect higher concentrations of highly incompatible elements (Cl, U, Nb, LREE and Sr) than the minerals in BFT137.

### Chemical reactions accompanying orthopyroxene growth

The modal proportions listed in Table 1 indicate that the following net mineralogical reaction took place, depending upon the choice of initial unreacted substrate:

BFT137 Matrix D as substrate:
1.25 Oliv + Fluid = 1 Opx + 0.076 Gar + 0.17 Phlog + 0.0086 Sulf + 0.038 Carb (1)
BFT147 as substrate:
1.15 Oliv + 0.05 Sp + Fluid = 1 Opx + 0.076 Gar + 0.13 Phlog + 0.0063 Sulf + 0.028 Carb (2)

In (1) and (2) the reaction coefficients are in terms of volume. The coefficient for carbonate was calculated assuming that all carbonate pseudomorphs in both vein and matrix were introduced during vein formation. This is probably a minimum, in that some introduced carbonate could have been deposited beyond the present boundary of the xenolith. Note that reaction (1) does not contain Cr-spinel (Sp) as a reactant because none is observed in the matrix to this xenolith. However, this does not mean it was not originally present; in fact it is likely, because our observations on a wider suite of refractory harzburgites indicate that Cr-spinel is common in harzburgites and dunites with Fo > 93.5. Reactions (1) and (2) are similar in their coefficients of reaction, indicating approximately one for one replacement of olivine by orthopyroxene, with other phases playing a much lesser role. The amount of fluid in the reaction cannot be constrained because the solute concentrations are unknown.

## Nature of the metasomatic agent

The very high Mg#, extremely low Ti, Ca and HREE contents of minerals, but presence of volatile-rich phases and high incompatible element concentrations in BFT137 indicate that a mafic or ultramafic silicate melt is an unlikely metasomatic agent. Reaction with such melts is commonly inferred for other mantle xenoliths, where it leads to prominent and distinctive Fe- and Ti-enrichment (Gurney and Harte 1980) and high HREE in garnet (Griffin et al. 1989; Burgess and Harte 1999). Mass balance considerations suggest that carbonatitic melt is unlikely to precipitate enstatite in significant quantities, although it may be in equilibrium with harzburgite at ~ 4 GPa (Lee and Wyllie 2000). The most likely candidate for the parent fluid therefore appears to be a hydrous siliceous fluid or melt, poor in ferromagnesian components, with minor but geochemically significant quantities of C and S.

The mineral assemblages and inferred reactions in BFT137 are consistent with the body of experimental results for the hybridization of hydrous, silica-rich melts or fluids with refractory peridotite (Sekine and Wyllie 1982; Wyllie et al. 1989; Rapp et al. 1999; Wunder and Melzer 2003). These studies show that enstatite, garnet, and phlogopite are the reaction products over a wide range of temperatures and pressures. However, the absence in BFT137 of Na-rich clinopyroxene, which is common in these hybridization experiments, suggests a metasomatic agent poor in Na and Ca. Whether the mobile phase was a dense hydrous supercritical fluid ("vapor") or a water-bearing siliceous melt is debatable. Experimental studies, reviewed by Wyllie and Ryabchikov (2000), indicate that a wide range of solute concentrations is possible as volatile-rich upper mantle systems approach a second critical endpoint in the P–T range from which our sample originates.

Understanding trace element partitioning as a function of volatile content may help to determine where the metasomatic agent fits in the fluid-melt spectrum. From their bulk chemical analyses of Kaapvaal xenoliths that indicated a lack of correlation between Re and Al, Carlson et al. (1999) favored a low-Al fluid rather than a siliceous melt such as a tonalite–trondhjemite for the metasomatic agent. This inference is based upon the assumption that Re, like Fe, would be less soluble in a fluid phase than a melt. The low Re content inferred for BFT137 from its low $^{187}Os/^{186}Os$ ratio is consistent with this interpretation. Furthermore, Stachel et al. (2004) argued that the REE patterns of harzburgitic garnets in xenoliths and diamond inclusions are qualitatively more consistent with fluids than melts.

## Composition of the added component

The bulk chemical changes that accompany orthopyroxene growth were calculated by assuming an appropriate starting composition and identifying a reference component unaffected by the metasomatic reaction. Two starting compositions were used; the BFT137 matrix, and sample BFT147. It is clear in BFT137 from textural evidence that some introduction of enstatite into the matrix occurred, and therefore this calculation yields a minimum estimate of the ensuing chemical change. BFT147 was chosen as a pre-metasomatic substrate because this sample has very similar bulk Mg# to BFT137 (93.8 vs. 93.9 for BFT137), but lacks major enstatite. Because the phlogopite is of likely metasomatic origin, the initial protolith composition was calculated without the $K_2O$ and $H_2O$ that are assumed to have been introduced into the xenolith. The choice of reference component is restricted in this study by the inference that diffusive re-equilibration of components after vein formation has occurred. The most suitable reference components are, therefore, those fixed by mineral stoichiometry, so long as the modes in vein and matrix have remained unchanged since their formation. We chose (Mg + Fe), which is approximately fixed by mineral stoichiometry in these low-Ca rocks.

Experimental studies at 1 – 4 GPa support the presumption of low Mg + Fe in upper mantle fluids and siliceous melts (Sekine and Wyllie 1982; Schneider and Eggler 1986; Brenan et al. 1995; Stalder et al.1998). However, the Mg content and Mg/Si of hydrous fluid in equilibrium with peridotite increase as a function of pressure (Stalder et al. 2001; Mibe et al. 2002), with < Mg/Si ~ 1 at 5–6 GPa.

The compositions of the added component calculated using the two starting compositions are reported in Table 7 and are similar. They show that the principal

**Table 7** Calculated composition of added component (wt.%)

| | A | B |
|---|---|---|
| $SiO_2$ | 80 | 83 |
| $Al_2O_3$* | 13 | 8.2 |
| CaO | 1.4 | 1.4 |
| $K_2O$ | 3.7 | 3.0 |
| $Na_2O$** | 0.45 | 0.40 |
| $H_2O$ | 1.5 | 1.2 |
| $SO_2$ | 0.68 | 0.54 |

1. Assumes BFT137 matrix as protolith, Mg + Fe as reference component
2. Assumes BFT147 (phlogopite-free) as protolith, Mg + Fe as reference component
* $Al_2O_3$ adjusted for post-formation Cr–Al exchange (see text)
** $Na_2O$ not adjusted for post-formation redistribution in opx and is therefore a minimum estimate

changes are in the Si and Al content of peridotite, with lesser amounts of added Ca, Na, K, H and S. Carbon is also added, but its abundance is not listed in table 7 because its distribution does not permit a clear distinction to be drawn between matrix and substrate. If all observed carbonate pseudomorphs were introduced during metasomatism, then about 4 wt.% $CO_2$ should be added to the composition listed in Table 7.

The $Na_2O$ and CaO contents listed in Table 7 are minimum values, because the Na and Ca introduced during metasomatism may have dissipated beyond the boundaries of the sampled xenolith during subsequent equilibration of mineral compositions with surrounding mantle. However, the overall low CaO and $Na_2O$ contents of the minerals suggest that this is not a major effect. For example, if all the Na in BFT137 was derived from the vein, the amount of $Na_2O$ estimated for the added component (0.4–0.5 wt.%, Table 7) would only increase by $\sim$ 0.5 wt.%. The Na content of the vein is unlikely to originally have been much higher because this would require Na contents in original orthopyroxene that exceed values measured in mantle samples. Therefore, we conclude that only limited quantities of Na and Ca were introduced. In the case of Al, a small correction was made to the nominal estimate based upon mass balance between vein and host, assuming that excess Cr in the vein had migrated into the vein during equilibration and was balanced by an equimolar quantity of Al that migrated out.

The composition of the added component is compared in Fig. 8 to those of various melts and fluids from experimental studies and of some glass inclusions in xenoliths from a mantle wedge environment. The composition of the added component is not likely to represent the bulk composition of a fluid or melt phase, or its anhydrous component, but rather the change in composition undergone by such a phase during its equilibration with the mantle. Fig. 8 shows that the added component is more Si-rich, and Al- and alkali-poor than melt inclusions in xenoliths (Schiano et al. 1995) and experimental siliceous liquids in equilibrium with olivine + orthopyroxene ± garnet ± phlogopite over a range

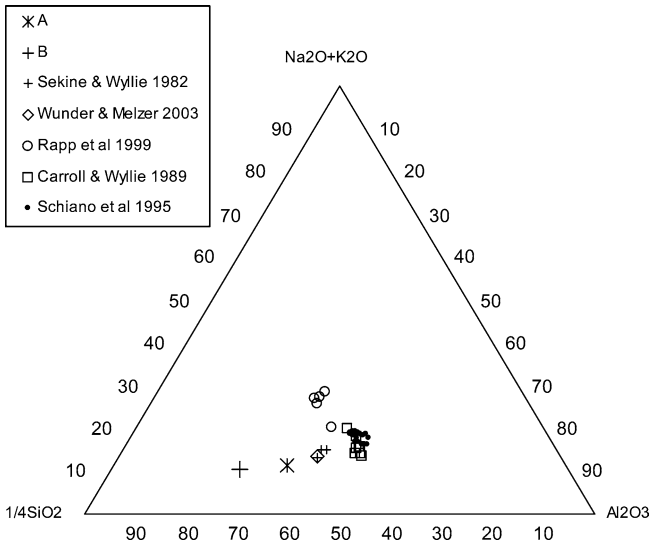


**Fig. 8** Composition of added component projected in the system $(Na_2O + K_2O) - Al_2O_3 - SiO_2$, compared with experimental liquids derived from the equilibration of granitoid compositions with peridotite at 1.5–3.7 GPa (see text for references), and with natural glass inclusions in peridotite xenoliths (Schiano et al. 1995). The letters A and B represent the compositions listed in Table 7

of upper mantle pressures (Sekine and Wyllie 1982, Carroll and Wyllie 1989, Johnston and Wyllie 1989, Rapp et al. 1999, Wunder and Melzer 2003). In particular, the added component is poor in Na in comparison to the experimental liquids and natural melt compositions from xenoliths. Natural granitoid magmas and siliceous liquids produced by melting hydrous basalt are Na-rich and produce a Na-rich reaction assemblage in hybridization experiments (Sekine and Wyllie 1982).

The Na-poor composition of the added component in BFT137 and the lack of clinopyroxene in the reaction assemblage indicate that the parental fluid or liquid differed from natural granitoid magmas or the primary melting products of subducted oceanic crust. A likely explanation for the difference is that the fluid or melt that interacted with BFT137 had already reacted substantially with the mantle. Garnet-phlogopite websterite assemblages are present (though not abundant) in the Bultfontein xenolith suite and attest to more Na-, Ca- and Al-rich reaction products in the general vicinity. Elsewhere, such assemblages have been linked to reaction of slab-derived melts (Aulbach et al. 2002). Sample BFT137 may therefore have been metasomatized by an evolved melt or dense hydrous fluid, derived from a siliceous melt that had undergone some prior reaction with the mantle to increase its $K_2O/Na_2O$, $SiO_2/Al_2O_3$, MgO/FeO and $(SiO_2 + Al_2O_3)/(CaO + Na_2O)$. This reaction would also alter the trace element signature of the fluid, leading, for example, to increasing LREE/HREE.

An alternative possibility that could account for the lack of Na and clinopyroxene in the reaction assemblage is that the parental fluid was formed by dehydration of

phengite in a subducting slab (Schmidt 1996, Domanik and Holloway 1996, Wunder and Melzer 2003), rather than by granitoid reaction-differentiation. Such fluids also react with peridotite to produce enstatite and phlogopite (Wunder and Melzer 2003). However, the presence of garnet in addition to phlogopite in the reaction products of BFT137 suggests molar $Al_2O_3/K_2O$ greater than that predicted for a fluid resulting from phengite breakdown to an anhydrous assemblage containing garnet and omphacite (Schmidt 1996). In order to discriminate conclusively between the possible compositions and genetic origins of the parental metasomatizing agent it may be necessary to quantify the full range of chemical changes found in the Kimberley xenoliths, and to assess their relative abundances.

## Geological setting of Kimberley metasomatism

Recent studies in the western Kaapvaal craton indicate that the Kimberley area from which our samples derive lies within a zone of Archean subduction and continental collision. Isotopic evidence from crustal zircons, peridotite xenoliths and diamond inclusions suggests convergence of eastern and western Kaapvaal blocks at 2.88 – 2.92 Ga, accompanied by mantle metasomatism, eclogite and diamond formation, and widespread later granitoid magmatism (Richardson et al. 2001; Shirey et al. 2002; Poujol et al. 2003; Schmitz et al. 2004). The evidence in BFT137 for mantle metasomatism by a volatile-rich siliceous fluid, as well as the geochemical characteristics inferred for this fluid, are consistent with the inferred proximity to a convergent plate boundary. Rb-Sr and Sm-Nd systematics of garnets suggest that the trace element enrichment in Kimberley harzburgites and diamond inclusions is Archean (Richardson et al. 1984, 1985), a conclusion supported by the large distances over which post-metasomatic chemical equilibrium was attained in sample BFT137.

The $T_{RD}$ of 2.97 ± 0.04 Ga for BFT137 is consistent with the proposed tectono-magmatic history of the Kimberley area. This minimum age may reflect melt depletion in the mantle wedge approximately contemporaneous with, or immediately prior to, collision. However, this age also permits mantle lithosphere formation in an earlier event as proposed by Griffin et al. (2004).

## Significance for cratonic mantle petrogenesis

Kesson and Ringwood (1989) suggested that orthopyroxene-rich peridotites of the Kaapvaal and other Archean cratons were formed by the reaction of silica dissolved in hydrous, slab-derived fluids with olivine to form enstatite. Mibe et al. (1998) demonstrated experimentally the feasibility of a porous flow mechanism for hydrous fluid metasomatism of the mantle at pressures greater than 3 GPa. This observation provides important support for the metasomatic hypothesis. Distinct veins of orthopyroxenite are not common within mantle xenolith suites from the Kaapvaal Craton and a metasomatic origin therefore requires a dispersed medium to account for the relatively uniform distribution of silica enrichment. The textural evidence in sample BFT137 is consistent with these proposals, and the chemical changes documented in this sample are consistent with the general sense in which Kaapvaal peridotites deviate from melting residue compositions (Walter 2004).

In a variation on this metasomatic theme, Rudnick et al. (1984) and Kelemen et al. (1998) proposed that siliceous melts, derived from the melting of a subducted slab could be the metasomatic agent. The textural evidence from BFT137 suggests that the metasomatic agent had very low viscosity. In order for a siliceous melt to attain sufficiently low viscosity to effectively percolate along grain boundaries as inferred in this particular case, high water content would be required. Complete miscibility between water-saturated melts and hydrous fluids for siliceous systems at pressures relevant to the present sample have been demonstrated (Shen and Keppler 1997; Bureau and Keppler 1999), and their low viscosities verified (Audétat and Keppler 2004). Sekine and Wyllie (1982) argued that hydrous melts would evolve to water saturation and evolution of hydrous fluid during their reaction with mantle peridotite. Thus, a continuum of melt-fluid compositions is likely to be generated during reactions of slab-derived mobile phases with overlying mantle, and the chemical and mineralogical features of individual xenolith samples should reflect this diversity.

A range of effects at different extents of fluid-rock reaction is also expected (Navon and Stolper 1987; Harte et al. 1983; Bodinier et al. 2004). In the olivine-rich garnet peridotite BFT147, the lack of orthopyroxene growth, but relative abundance of phlogopite with a tenfold increase in Cl content over that observed in the enstatite-rich veined sample, provides possible evidence of such compositional evolution in the fluid. The garnet of this sample is also enriched in the highly incompatible elements (U, Nb, Sr, LREE) relative to BFT137.

The occurrence of sulfides and carbonate pseudomorphs in BFT137 suggests that significant quantities of $CO_2$ and S could have been introduced into the lithospheric mantle by subduction–derived fluids. Reduction of $CO_2$ and $SO_2$ to sulfide and graphite or diamond provides a mechanism to oxidize the lithospheric mantle. The restriction of sulfide to the vein itself suggests that it may have been fixed rapidly by reaction of fluid-derived $SO_2$ or sulfate with FeO in the matrix minerals.

Although sample BFT137 likely represents one stage in a continuum of metasomatic products, its representativeness for the Kaapvaal cratonic mantle as a whole may be evaluated by considering that the $SiO_2/K_2O$ ratio of the added component (using data from Table 7) is 25 ± 3. If it is assumed that the difference in $SiO_2$ content of average Kaapvaal low-temperature peridotite (46.6 wt.% - Boyd 1989) was all derived by metasoma-

tism of a protolith resembling the BFT137 matrix, or the olivine-rich sample BFT147, by the reactions discussed above, then a metasomatic $K_2O$ content in the range 0.085 – 0.25 wt.% is implied. Such estimates are in the range of average measured $K_2O$ contents of Kaapvaal peridotites, but are not easily reconciled with thermal constraints that require low mantle heat production (Rudnick et al. 1998). This suggests that the sample examined here represents a particularly K-rich part of the reaction process, supporting arguments above for a relatively evolved fluid and the existence elsewhere of less K-rich siliceous reaction products.

By studying a wider range of metasomatic reaction products and determining their stratigraphic position in the mantle by thermobarometry, the Kimberley xenolith suite and others from surrounding mantle offer a potential opportunity to reconstruct details of an ancient subduction zone and provide important constraints on Archean tectonic processes and geochemical cycles. Recognizing and accounting for metasomatic effects in the bulk compositional trends of cratonic peridotites should also permit a more reliable assessment of the conditions under which the primary melt depletion was acquired. The results of this study are consistent with models for cratonic lithosphere generation in a subduction zone setting (Kesson and Ringwood 1989, Parman et al. 2004) but do not address directly the question of where primary melt depletion occurred. However, indications that metasomatism decreases the Cr/Al ratio of cratonic peridotite strengthens arguments for melting within the stability field of spinel (Kesson and Ringwood 1989, Stachel et al. 1998).

## Summary

The veined harzburgite xenolith BFT137 from Kimberley provides evidence for metasomatic introduction of Si, Al, K, H, C and S into the cratonic mantle. The metasomatic agent is inferred to be a hydrous fluid rich in silica, which had evolved by prior reaction with surrounding mantle. The parent to this fluid originated in oceanic lithosphere, subducted during convergence between eastern and western blocks of the Kaapvaal Craton at $\sim$ 2.9 Ga. Trace element enrichment patterns in garnet are qualitatively similar to others from Kaapvaal xenoliths and suggest that the pervasive trace element enrichment of the Kaapvaal mantle is effected by fluids similar to those inferred here. These results imply that subduction processes played an important role in modifying the composition of Archean SCLM.

**Acknowledgments** This work was supported by US National Science Foundation grants EAR-9526702, EAR-9526840, EAR-0003533 and EAR-0310330. DRB gratefully acknowledges support at MIT from a Crosby Fellowship. We thank Sam Bowring (MIT) for discussions, Anton le Roex (University of Cape Town) for hosting the ICP-MS analyses in his laboratory, the Carnegie Institution of Washington for access to electron microprobe facilities, and De Beers Consolidated Mines for field support and permission to sample the Kimberley dumps.

## References

Anders E, Grevesse N (1989) Abundances of the elements: meteoritic and solar. Geochim Cosmochim Acta 53: 197–214

Audétat D, Keppler H (2004) Viscosity of fluids in subduction zones. Science 303: 513–516

Aulbach S, Stachel T, Viljoen KS, Brey GP, Harris JW (2002) Eclogitic and websteritic diamond sources beneath the Limpopo belt – is slab melting the link. Contrib Mineral Petrol 143: 56–70

Bell DR, Grégoire M, Grove TL, Chatterjee N, Bowring, SA (2003) Silica and carbon deposition in the Kimberley peridotites. Extd Abstr 8th International Kimberlite Conf Victoria Canada, 4 pp (unpaginated CD)

Berg GW (1986) Evidence for carbonate in the mantle. Nature 324: 50–51

Bodinier J-L, Menzies MA, Shimizu N, Frey FA, McPherson E (2004) Silicate, hydrous and carbonate metasomatism at Lherz, France: contemporaneous derivatives of silicate melt – harzburgite reaction. J Petrol 45: 299–320

Boyd FR (1989) Compositional distinction between oceanic and cratonic lithosphere. Earth Planet Sci Lett 96: 15–26

Boyd FR, McCallister RH (1976) Densities of fertile and sterile garnet lherzolites. Geophys Res Lett 3: 509–512

Boyd FR, Mertzman SA (1987) Composition and structure of the Kaapvaal lithosphere. In: Mysen BO (ed) Magmatic processes: Physicochemical principles. Geochemical Society Spec Publ 1: 13–24

Boyd FR, Pokhilenko NP, Pearson DG, Mertzman SA, Sobolev NV, Finger LW (1997) Composition of the Siberian cratonic mantle: evidence from Udachnaya peridotite xenoliths. Contrib Mineral Petrol 128: 228–246

Brenan JM, Shaw HF, Ryerson FJ, Phinney DL (1995) Mineral-aqueous fluid partitioning of trace elements at 900°C and 20 GPa: constraints on the trace element chemistry of mantle and deep crustal fluids. Geochim Cosmochim Acta 59: 3331–3350

Brey GP, Köhler T (1990) Geothermobarometry in four phase lherzolites II. New thermobarometers and practical assessment of existing thermobarometers. J Petrol 31: 1353–1378

Bureau H, Keppler H (1999) Complete miscibility between silicate melts and hydrous fluids in the upper mantle: experimental geochemical evidence and geochemical implications. Earth Planet Sci Lett 165: 187–196

Burgess SR, Harte B (1999) Tracing lithosphere evolution through the analysis of heterogeneous G9/G10 garnets in peridotite xenoliths, I: major element chemistry. In: Gurney JJ, Gurney JL, Pascoe MD, Richardson SH (eds) The J.B. Dawson Volume. Proc 7thInternat Kimberlite Conf, Red Roof Design, Cape Town, pp 66–80

Canil D (1991) Experimental evidence for the exsolution of cratonic peridotite from high-temperature harzburgite. Earth Planet Sci Lett 106: 64–72

Carlson RW, Moore RO (2004) Age of the eastern Kaapvaal mantle: Re-Os isotope data for peridotite xenoliths from the Monastery kimberlite. S Afr J Geol 107: 81–90

Carlson RW, Pearson DG, Boyd FR, Shirey SB, Irvine G, Menzies AH, Gurney JJ (1999) Re-Os systematics of lithospheric peridotites: implications for lithosphere formation and preservation. In: Gurney JJ, Gurney JL, Pascoe MD, Richardson SH (eds) The J. B. Dawson Volume Proc 7th Internat Kimberlite Conf. Red Roof Design, Cape Town, pp 99–108

Carroll MR, Wyllie P J (1989) Experimental phase relations in the system peridotite – tonalite – $H_2O$ at 15 kbar; implications for assimilation and differentiation processes near the crust mantle boundary. J Petrol 30: 1351–1382

Cox KG, Smith MR and Beswetherick S (1987) Textural studies of garnet lherzolites: evidence of exsolution origin from high-temperature harzburgites. In Nixon PH (ed) Mantle Xenoliths. John Wiley and Sons, Chichester, pp 537–550

Dawson JB (2004) A fertile harzburgite to garnet lherzolite transition: possible inferences for the roles of strain and metasomatism in upper mantle peridotites. Lithos 77: 553–570

Dawson JB, Stephens WE (1975) Statistical classification of garnets from kimberlite and associated xenoliths. J Geol 83: 589–607

Domanik KJ, Holloway JR (1986) The stability and composition of phengitic muscovite and associated phases from 5.5 to 11 GPa: implications for deeply subducted sediments. Geochim Cosmochim Acta 60: 4133–4150

Erlank AJ, Waters FG, Hawkesworth CJ, Haggerty SE, Allsopp HL, Rickard RS, Menzies M (1987) Evidence for mantle metasomatism in peridotite nodules from the Kimberley pipes, South Africa. In: Menzies M, Hawkesworth CJ (eds) Mantle metasomatism. Academic Press, London, pp 221–309

Gaul O, Griffin WL, O'Reilly SY, Pearson NJ (2000) Mapping olivine composition in the lithospheric mantle. Earth Planet Sci Lett 182: 223–235

Grégoire M, Bell DR, le Roex AP (2002) Trace element geochemistry of phlogopite-rich mafic xenoliths: their classification and their relationship to phlogopite-bearing peridotites and kimberlites revisited. Contrib Mineral Petrol 142: 603–625

Grégoire M, Bell DR, le Roex AP (2003) Garnet lherzolites from the Kaapvaal Craton (South Africa): trace element evidence for a metasomatic history. J Petrol 44: 629–657

Griffin WL, Smith D, Boyd FR, Cousens DR, Ryan CG, Sie SH, Suter GF (1989) Trace element zoning in garnets from sheared mantle xenoliths. Geochim Cosmochim Acta 53: 561–567

Griffin WL, O'Reilly SY, Ryan CG (1999) The composition and origin of the sub-continental lithospheric mantle. In: Fei Y, Bertka CM, Mysen BO (eds) Mantle petrology: field observations and high pressure experimentation: a tribute to Francis R. (Joe) Boyd. Geochemical Soc Spec Publ 6: 13–45

Griffin WL, O'Reilly SY, Abe N, Aulbach S, Davies RM, Pearson NJ, Doyle BJ, Kivi K (2003) The origin and evolution of Archean lithospheric mantle. Precambrian Res 127: 19–41

Griffin WL, Graham S, O'Reilly SY, Pearson NJ (2004) Lithosphere evolution beneath the Kaapvaal Craton: Re-Os systematics of sulfides in mantle-derived peridotites. Chem Geol 208: 89–118

Gurney JJ (1984) A correlation between garnets and diamonds. In: Glover JE, Harris PG (eds) Kimberlite occurrence and origin: a basis for conceptual models in exploration. Geology Dept and University Extension, University of Western Australia Publ 8: 143–166

Gurney JJ, Harte B (1980) Chemical variations in upper mantle nodules from southern African kimberlites. Phil Trans Royal Soc London A297: 273–293

Harte B, Hunter RH, Kinny PD (1993) Melt geometry, movement and crystallization, in relation to mantle dykes, veins, and metasomatism. Phil Trans R Soc Lond A342: 1–21

Herzberg C (1993) Lithosphere peridotites of the Kaapvaal craton. Earth Planet Sci Lett 120: 13–29

Hoal KEO, Hoal BG, Erlank AJ, Shimizu N (1994) Metasomatism of the mantle lithosphere recorded by rare-earth elements in garnet. Earth Planet Sci Lett 126: 303–313

Hops JJ, Gurney JJ, Harte B, Winterburn P (1989) Megacrysts and high temperature nodules from the Jagersfontein kimberlite pipe. In : Ross J et al (eds) Kimberlites and Related rocks. Volume 2. Their mantle/crust setting, diamonds and diamond exploration. Geol Soc Australia Spec Publ 14: 759–770

Johnston AD, Wyllie PJ (1989) The system tonalite-peridotite-$H_2O$ at 30 kbar, with applications to hybridization in subduction zone magmatism. Contrib Mineral Petrol 102: 257–264

Jones AP, Smith JV, Dawson, JB (1982) Mantle metasomatism in 14 veined peridotites from Bultfontein mine, South Africa. J Geol 90: 435–453

Jordan TH (1988) Structure and formation of the continental tectosphere. Journal of Petrology Special Lithosphere Issue: 11–37

Kelemen PB (1990) Reaction between ultramafic wallrock and fractionating basaltic magma Part I Phase relations, the origin of calc-alkaline magma series and the formation of discordant dunite. J Petrol 31: 51–98

Kelemen PB (1995) Generation of high-Mg andesites and the continental crust. Contrib Mineral Petrol 120: 1–19

Kelemen PB, Shimizu N, Dunn JT (1993) Relative depletion of niobium in some arc magmas and the continental crust: partitioning of K, Nb, La and Ce during melt/rock reaction in the upper mantle. Earth Planet Sci Lett 120: 111–133

Kelemen PB, Hart SR, Bernstein S (1998) Silica enrichment in the continental upper mantle via melt/rock reaction. Earth Planet Sci Lett 164: 387–406

Kepezhinskas PK, Defant MJ, Drummond MS (1995) Na metasomatism in the island-arc mantle by slab melt – peridotite interaction: evidence from mantle xenoliths in the North Kamchatka arc. J Petrol 36: 1505–1527

Kepezhinskas PK, Defant MJ, Drummond MS (1996) Progressive enrichment of island arc mantle by melt-peridotite interaction inferred from Kamchatka xenoliths. Geochim Cosmochim Acta 60: 1217–1229

Kesson SE, Ringwood AE (1989) Slab – mantle interactions. 2. The formation of diamonds. Chem Geol 78: 97–118

Kinzler RJ, Grove TL (1999) Origin of depleted cratonic harzburgite by deep fractional melt extraction and shallow olivine cumulate infusion. In Gurney JJ, Gurney JL, Pascoe MD, Richardson SH (eds) The J.B. Dawson Volume. Proc 7th Internat Kimberlite Conf. Red Roof Design, Cape Town, pp 437–443

Kopylova MG, Russell JK (2000) Chemical stratification of cratonic lithosphere: constraints from the Northern Slave Craton, Canada. Earth Planet Sci Lett 181: 71–87

Kramers JD Roddick JCM, Dawson JB (1983) Trace element and isotopic studies on veined, metasomatic and "MARID" xenoliths from Bultfontein. South Africa Earth Planet Sci Lett 65: 90–106

Lahaye Y, Brey GP (2003) Scale and timing constraints on chemical redistribution between minerals of a composite garnet peridotite/orthopyroxenite. Abstr 8th Internat Kimberlite Conf Victoria, Canada, CD unpaginated

Laurora A, Mazzucchelli M, Rivalenti G, Vannucci R, Zanetti A, Barbier MA, Cingolani C (2001) Metasomatism and melting in carbonated peridotite xenoliths for the mantle wedge: the Gobernador Gregores case (southern Patagonia). J Petrol 42: 69–87

Lee WJ, Wyllie PJ (2000) The system CaO-MgO-$SiO_2$-$CO_2$ at 1 GPa, metasomatic wehrlites, and primary carbonatite magmas. Contrib Mineral Petrol 138: 214–228

Lorand JP (1993) Comment on 'Content and isotopic composition of sulphur in ultramafic xenoliths from central Asia' by D. A. Ionov, J. Hoefs, K. H. Wedepohl and U. Wiechert. Earth Planet Sci Lett 119: 627–634

McDonough WF, Sun S (1995) The composition of the Earth. Chem Geol 120: 223–253

McInnes BIA, Cameron EM (1994) Carbonated, alkaline hybridizing melts from a sub-arc environment: mantle wedge samples from the Tabar-Lihir-Feni arc, Papua New Guinea. Earth Planet Sci Lett 122: 125–141

McInnes BIA, Grégoire M, Binns RA, Herzig PM, Hannington MD (2001) Hydrous metasomatism of oceanic sub-arc mantle, Lihir, Papua New Guinea: petrology and geochemistry of fluid-metasomatised mantle wedge xenoliths. Earth Planet Sci Lett 188: 169–183

Mibe K, Fujii T, Yasuda A (1998) Connectivity of aqueous fluid in the Earth's upper mantle. Geophys Res Lett 25: 1233–1236

Mibe K, Fujii T, Yasuda A (2002) Composition of aqueous fluid coexisting with mantle minerals at high pressure and its bearing on the differentiation of the Earth's mantle. Geochim Cosmochim Acta 66: 2273–2285

Navon O, Stolper EM (1987) Geochemical consequences of melt percolation: the upper mantle as a chromatographic column. J Geol 95: 285–307

Niu Y, Langmuir CH and Kinzler RJ (1997) The origin of abyssal peridotites; a new perspective. Earth Planet Sci Lett 152: 251–265

O'Hara MJ, Saunders MJ, Mercy, ELP (1975) Garnet-peridotite primary ultrabasic magma and eclogite; interpretation of the upper mantle process in kimberlite. Phys Chem Earth 9: 571–604

O'Neill HS (1980) An experimental study of Fe-Mg partitioning between garnet and olivine and its calibration as a geothermometer: corrections. Contrib Mineral Petrol 72: 337

O'Neill HS, Wood BJ (1979) An experimental study of Fe-Mg partitioning between garnet and olivine and its calibration as a geothermometer. Contrib Mineral Petrol 70: 59–70

Parman SW, Grove TL, De Wit MJ, Dann JC (2004) A subduction origin for komatiites and cratonic lithospheric mantle. S Afr J Geol 107: 107–118

Pearson DG, Carlson RW, Shirey SB, Boyd FR, Nixon PH (1995a) Stabilisation of Archaean lithospheric mantle; a Re-Os isotope study of peridotite xenoliths from the Kaapvaal Craton. Earth Planet Sci Lett 134: 341–357

Pearson DG, Shirey SB, Carlson RW, Boyd FR, Pokhilenko NP, Shimizu N (1995b) Re-Os, Sm-Nd, and Rb-Sr isotope evidence for thick Archaean lithospheric mantle beneath the Siberian craton modified by multistage metasomatism. Geochim Cosmochim Acta 59: 959–977

Pokhilenko NP, Sobolev NV, Boyd FR, Pearson DG, Shimizu N (1993) Megacrystalline pyrope peridotites in the lithosphere of the Siberian Platform; mineralogy, geochemical peculiarities and the problem of their origin. Russian Geol Geophys 34: 56–67

Poujol M, Robb LJ, Annhaeusser CJ, Gericke B (2003) A review of the geochronological constraints on the evolution of the Kaapvaal Craton, South Africa. Precambrian Res 127: 181–213

Prouteau G, Scaillet B, Pichavant M, Maury R (2001) Evidence for mantle metasomatism by hydrous silicic melts derived from subducted crust. Nature 410: 197–200

Rapp RP, Shimizu N, Norman MD, Applegate GS (1999) Reaction between slab-derived melts and peridotite in the mantle wedge: experimental constraints at 38 GPa. Chem Geol 160: 335–356

Richardson SH, Gurney JJ, Erlank AJ, Harris JW (1984) Origin of diamonds in old enriched mantle. Nature 310: 198–202

Richardson SH, Erlank AJ, Hart SR (1985) Kimberlite-borne garnet peridotite xenoliths from old enriched subcontinental lithosphere. Earth Planet Sci Lett 75: 116–128

Richardson SH, Shirey S B, Harris JW, Carlson RW (2001) Archean subduction recorded by Re-Os isotopes in eclogitic sulfide inclusions in Kimberley diamonds. Earth Planet Sci Lett 191: 257–266

Rudnick RL, McDonough WF, Orpin A (1994) Northern Tanzanian peridotite xenoliths: a comparison with Kaapvaal peridotites and inferences on metasomatic interactions. In: Meyer HOA, Leonardos O (eds) Kimberlites, related rocks and mantle xenoliths, Vol 1 Proc 5th Internat Kimberlite Conf CPRM Brasilia pp 336–353

Rudnick RL, McDonough WF, O'Connell RJ (1998) Thermal structure, thickness and composition of continental lithosphere. Chem Geol 145: 395–411

Saltzer RL, Chatterjee N, Grove TL (2001) The spatial distribution of garnets and pyroxenes in mantle peridotites; pressure-temperature history of peridotites from the Kaapvaal Craton. J Petrol 42:2215–2229

Schiano P, Clochiatti R, Shimizu N, Maury RC, Jochum KP, Hoffman AW (1995) Hydrous, silica rich melts in the sub-arc mantle and their relationship with erupted arc lavas. Nature 377: 595–600

Schmidt MW (1996) Experimental constraints on recycling of potassium from subducted oceanic crust. Science 270: 625–627

Schmitz MD, Bowring SA, de Wit MJ, Gartz V (2004) Neoarchean continent collision in the western Kaapvaal craton, southern Africa and its implications for the stabilization of continental lithosphere. Earth Planet Sci Lett 222: 363–376

Schneider M E, Eggler D H (1986) Fluids in equilibrium with peridotite minerals: implications for mantle metasomatism. Geochim Cosmoschim Acta 50: 711–724

Sekine T, Wyllie PJ (1982) The system granite – peridotite – $H_2O$ at 30 kbar, with applications to hybridization in subduction zone magmatism. Contrib Mineral Petrol 81: 190–202

Shapiro SS, Hager B H, Jordan T H (1999) Stability and dynamics of the continental tectosphere. Lithos 48: 115–133

Shen AH, Keppler H (1997) Direct observation of complete miscibility on the albite-$H_2O$ system. Nature 385: 710–712

Shimizu N (1975) Rare earth elements in garnets and clinopyroxenes from garnet lherzolite nodules in kimberlites. Earth Planet Sci Lett 25: 26–32

Shimizu N, Richardson SH (1987) Trace element abundance patterns of garnet inclusions in peridotite-suite diamonds. Geochim Cosmochim Acta 51: 755–758

Shimizu N, Pokhilenko NP, Boyd FR, Pearson DG (1999) Trace element characteristics of garnet dunites/harzburgites, host rocks for Siberian peridotitic diamonds. Gurney JJ, Gurney JL, Pascoe MD, Richardson SH (eds) The P.H. Nixon Volume Proc 7th Internat Kimberlite Conf. Red Roof Design, Cape Town, pp 773–782

Shirey SB, Harris JW, Richardson SH, Fouch MJ, James DE, Cartigny P, Deines P, Viljoen F (2002) Diamond genesis, seismic structure, and evolution of the Kaapvaal-Zimbabwe Craton. Science 297: 1683–1686

Simon NSC, Irvine GJ, Davies GR, Pearson DG, Carlson RW (2003a) The origin of garnet and clinopyroxene in "depleted" Kaapvaal peridotites. Lithos 71: 289–322

Simon NSC, Carlson R W, Davies G R, Nowell G M, Pearson D G (2003b) Os-Sr-Nd-Hf isotope evidence for the ancient depletion and subsequent multistage enrichment history of the Kaapvaal cratonic lithosphere Extd Abstrs 8th Internat Kimberlite Conf Victoria Canada, CD unpaginated

Smith D (2000) Insights into the evolution of the uppermost continental mantle from xenolith localities on and near the Colorado Plateau and regional comparisons. J Geophys Res 105: 16,769–16,781

Smith D, Riter JCA, Mertzman SA (1999) Water-rock interactions, orthopyroxene growth, and Si-enrichment in the mantle: evidence in xenoliths from the Colorado Plateau, southwestern United States. Earth Planet Sci Lett 165: 45–54

Smith D, Connelly JN, Manser K, Moser D, Housh T, McDowell F, Mack LE (2004) Evolution of Navajo eclogites and hydration of the mantle below the Colorado Plateau, southwestern United States. Geochem Geophys Geosystems 5 (4): Q04005 doi:10.1029/2003GC000675

Stachel T, Viljoen KS, Brey GP, Harris JW (1998) Metasomatic processes in lherzolitic and harzburgitic domains of diamondiferous lithospheric mantle: REE in garnets from xenoliths and inclusions in diamonds. Earth Planet Sci Lett 159: 1–12

Stachel T, Harris JW, Brey GP (1999) REE patterns of peridotitic and eclogitic inclusions in diamonds from Mwadui (Tanzania). In. Gurney JJ, Gurney JL, Pascoe MD, Richardson SH (eds) The NixonVolume Proc 7th Internat Kimberlite Conf, Red Roof Design, Cape Town, pp 829–835

Stachel T, Aulbach S, Brey GP, Harris JW, Leost I, Tappert R, Viljoen KS (2004) The trace element composition of silicate inclusions in diamonds: a review. Lithos 77:1–21

Stalder R, Foley SF, Brey GP, Horn I (1998) Mineral-aqueous fluid partitioning of trace elements at 900–1200°C and 30–57 GPa: new experimental data for garnet, clinopyroxene, and rutile, and implications for mantle metasomatism. Geochim Cosmochim Acta 62: 1781–1801

Stalder R, Ulmer P, Thompson AB, Günther D (2001) High pressure fluids in the system $MgO$-$SiO_2$-$H_2O$ under upper mantle conditions. Contrib Mineral Petrol 140: 607–618

Tomoaki M, Arai S, Green DH (2003) Evolution of low-Al orthopyroxene in the Horoman Peridotite Japan; an unusual indicator of metasomatizing fluids. J Petrol 44: 1237–1246

Wagner TP, Grove TL (1998) Melt/harzburgite reaction in the petrogenesis of tholeiitic magma from Kilauea Volcano, Hawaii. Contrib Mineral Petrol 131: 1–12

Walker RJ, Carlson RW, Shirey SB, Boyd FR (1989) Os, Sr, Nd, and Pb isotope systematics of southern African peridotite xenoliths: implications for the chemical evolution of subcontinental mantle. Geochim Cosmochim Acta 53: 1583–1595

Walter MJ (1998) Melting of garnet peridotite and the origin of komatiite and depleted lithosphere. J Petrol 39: 29–60

Walter MJ (1999) Melting residues of fertile peridotite and the origin of cratonic lithosphere. In Fei Y, Bertka CM, Mysen BO (eds) Mantle petrology: field observations and high pressure experimentation: a tribute to Francis R (Joe) Boyd Geochemical Soc Spec Publ 6: 225–239

Walter MJ (2004) Melt extraction and compositional variability in mantle lithosphere. In: Carlson RW (ed) The Mantle and Core, Vol 2 Treatise on Geochemistry (eds HD Holland and KK Turekian), Elsevier-Pergamon, Oxford, pp 363–394

Wunder B, Melzer S (2003) Experimental evidence on phlogopite mantle metasomatism induced by phengite dehydration. Eur J Mineral 15: 641–647

Wyllie PJ, Carroll MR, Johnston AD, Rutter MJ, Sekine T, Van der Laan SR (1989) Interactions among magmas and rocks in subduction zone regions: experimental studies from slab to mantle to crust. Eur J Mineral 1: 165–179

Wyllie PJ, Ryabchikov ID (2000) Volatile components, magmas, and critical fluids in upwelling mantle. J Petrol 41: 1195–1206

Zanetti A, Mazzucchelli M, Rivalenti G, Vannucci R (1999) The Finero phlogopite-peridotite massif: an example of subduction-related metasomatism. Contrib Mineral Petrol 134: 107–122